Supporting Information

Designer Dual Therapy Nanolayered Implant Coatings Eradicate Biofilms and Accelerate Bone Tissue Repair

*Jouha Min,[1,2] Ki Young Choi,[1,2] Erik C. Dreaden,[1,2] Robert F. Padera,[3,4] Richard D. Braatz,[1] Myron Spector,[3,5,6] Paula T. Hammond[1,2]**

[1]Department of Chemical Engineering, Massachusetts Institute of Technology, Cambridge, Massachusetts, 02139 USA

[2]Koch Institute for Integrative Cancer Research, Massachusetts Institute of Technology, Cambridge, Massachusetts, 02139 USA

[3]The Harvard-MIT Division of Health Sciences and Technology, Massachusetts Institute of Technology, Cambridge, Massachusetts, 02139 USA.

[4]Department of Pathology, Brigham and Women's Hospital, Boston, Massachusetts, 02215 USA

[5]Department of Orthopedic Surgery, Brigham and Women's Hospital, Boston, Massachusetts, 02115 USA

[6]Tissue Engineering Laboratories, VA Boston Healthcare System, Boston, Massachusetts, 02130 USA

* Corresponding author. Email: hammond@mit.edu

The PDF file includes

Methods

Fig. S1. Determination of minimum inhibitory concentration (MIC) of gentamicin against *S. aureus* Xen 29.

Fig. S2. Biocompatibility of the dual therapy multilayer coatings in uninfected rats.

Fig. S3. Surface morphology of LbL coatings on drilled PEEK implants.

Fig. S4. Predicted concentration of GS and BMP-2 in bone.

Fig. S5. Release kinetics and *in vitro* biological evaluation.

Fig. S6. *In vitro* bioactivity evaluation.

Fig. S7. Development of implant-related chronic osteomyelitis *via* direct inoculation method.

Fig. S8. Bacterial resistance against GS after explantation.

Fig. S9. Histological examination of excised tibiae treated with different coating formulations.

Fig. S10. Mature bone formation around implants coated with dual therapy films.

Fig. S11. Arrangement of new bone on uncoated and Dual therapy coated implants at 8 weeks post-revision**.**

Fig. S12. Reinfection after revision in untreated rats.

Fig. S13. New bone formation in medullary canal over time.

Fig. S14. New bone formation around and inside the drilled implants.

Table S1. Interfacial shear strength of implants coated with different film formulations.

Methods

Release characterization. Films with protein (rhBMP-2) and antibiotic (GS + ^{3}H-GS) were immersed into 1 mL of phosphate buffer solution (PBS) with pH 7.4 in a capped 2-mL micro-centrifuge tube maintained at 37 ˚C. At predetermined time points, 0.5 mL of sample was collected from the tube and replaced with 0.5 mL of pre-warmed PBS. This process was performed in a gentle manner such that it does not cause any mechanical disturbance to the films. Samples were stored at –20 ˚C until analyzed. The samples from consecutive time points were then analyzed by bacterial and/or cellular assays (see below).

For rhBMP-2 quantification, an ELISA development kit (Peprotech Inc., Rocky Hill, NJ) was used. For GS, each 0.5 mL sample was then mixed with 5 mL of ScintiSafe Plus 50% (Fisher Scientific, Atlanta, GA) prior to the quantification. The mixtures are analyzed using a Tricarb Model 2810 TR liquid scintillation counter (Perkin Elmer, Waltham, MA). The raw data given in disintegrations per minute (DPM) is converted to the mass of GS by using a calibration curve of [concentration versus DPM], which is linear over the GS concentration range used in this study. The total cumulative GS released from the film at a given time point (i) can be calculated by

$$m_i = C_i V_i + (0.5\ \text{mL}) \sum_{j=1}^{i-1} C_j$$

where m_i (μg) is the total cumulative amount of GS released at time point (i), C_i (μg/mL) is the concentration of sample i, V_i (mL) is the total volume of the release medium, and the summation term adds up the total extensive quantity of GS removed in each of the previous aliquots.

***S.aureus* antimicrobial susceptibility assays.** The efficacy of GS loaded on the LbL films was evaluated by exploring the activity of the LbL films directly as well as drug release solutions using the previously described methods. Briefly, the LbL film activity was assessed directly using a Kirby-Bauer disk diffusion assay on a bacteria-coated agar plate. Agar plates were inoculated with exponentially growing *S.aureus* in cation-adjusted Mueller Hinton broth (CMHB) at 10^{8} CFU/mL and incubated at 37 ˚C for 16–18 h. The diameter of inhibition zone was measured in millimeters.

A quantitative determination of GS activity from the LbL films was obtained according to a previously published microdilution procedure [39] in CMHB with an inoculation of 10^{5} CFU/mL.

The 96-well clear bottom plate was incubated at 37 ˚C for 16–18 h and read at 600 nm in a Tecan Infinite® 200 PRO microplate reader. Normalized bacteria inhibition was calculated using

$$\text{Normalized S. aureus density} = \frac{OD_{600,\text{sample}} - OD_{600,\text{negative control}}}{OD_{600,\text{positive control}} - OD_{600,\text{negative control}}}$$

Cell culture. To determine the efficacy of the release of growth factors from the LbL films and the cytotoxic effect of the films, *in vitro* tests were performed to quantify and visualize the effects on pre-osteoblast cell line MC3T3-E1 with high osteoblast differentiation and mineralization activity. rhBMP-2 initiates the differentiation of pre-osteoblast MC3T3-E1 into bone.

MC3T3-E1 cells were cultured in growth medium (α-MEM supplemented with 10% FBS and 1% of antibiotic and antimycotic solution) in a humidified incubator (37 ˚C; 5% CO_2 in air). Growth medium was replenished every 2–3 days and cells were subcultured when near 100% confluence with the use of 0.05% trypsin-EDTA. All cells used in these studies were less than passage number 12.

Elution buffers were prepared by incubating each LbL film in 2 mL of growth medium at 37 ˚C. At predetermined time points, the release media was replaced with pre-warmed media. The extracted samples were stored at –20 ˚C until analyzed.

Cells were seeded at a density of 10^4 cells/cm^2 in the wells of 6-well or 12-well tissue culture plates (Corning) and incubated at 37 ˚C and 5% CO_2 in humidified air for 24–48 h prior to exposure to delivery platforms containing rhBMP-2 or elution buffers in cellular assays. Each delivery platform containing rhBMP-2 was placed on a culture insert (Transwell®, Corning) in the culture plate. The growth medium was changed to growth medium or differentiation medium (growth medium supplemented with 10 mM of β-glycerol phosphate and 50 mg/mL of L-ascorbic acid) and incubated with the plated MC3T3-E1 cells prior to evaluation.

Alkaline phosphatase activity assay. Alkaline phosphatase (ALP) activity was measured on day 6 after the initiation of MC3T3-E1 osteogenic differentiation using the Alkaline Phosphatase Colorimetric Assay kit (Abcam), which quantifies the ALP enzyme activity. The assay was performed according to the manufacturer's specifications. The ALP activity measurements were then normalized to total protein determined by BCA assay (Pierce). For colorimetric ALP detection, NBT (nitro-blue tetrazolium chloride) and BCIP (5-bromo-4-chloro-3'-indolyphosphate p-toluidine salt) substrate solution (Pierce) was incubated with cells for 20 min at 37 ˚C. Cells were then washed in DI water, and the stained cultures were visualized under phase contrast microscopy.

Co-culture of preosteoblast cells and bacteria. Bacterial cells *S. aureus* were taken from a growing liquid culture and incubated in LB medium at 37 ˚C for 16–18 h. The culture was centrifuged (10 min at 4,300 g and 4 ˚C) and the pellet was washed with PBS and resuspended in 10 mL of differential media. MC3T3-E1 cells at a density of 10^4 cells/cm^2 were cultured and grow overnight. The cell cultures were infected with the bacterial suspension for an approximate final concentration of 10^7 CFU/mL. The bacterial concentration is higher than that used for monocultures in order to aid in the differentiation of treatment groups by using a more stringent set of conditions. This co-culture was then incubated for 45 minutes at 37 ˚C. The cell culture wells were aspirated and washed with PBS to remove the extracellular bacteria and incubated with the films or treatment combination solutions (GS and/or BMP2).

S. aureus Xen 29

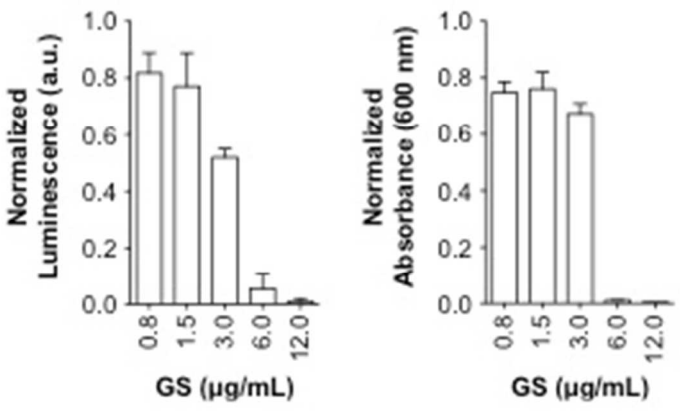

Fig. S1. Determination of minimum inhibitory concentration (MIC) of gentamicin against *S. aureus* Xen 29. Minimum normalized *S. aureus* Xen 29 density upon exposure to serial dilutions of naked GS was measured using bioluminescent imaging (left) and microplate reader at 600 nm (right). MIC is ~6 µg/mL. Data represent the mean ± s.e.m., *n* = 3.

The luciferase encoding *S. Aureus* Xen 29 used in this study has 20-fold higher antibiotic resistance against GS than general strains of *S. aureus* (0.25 µg/mL < $MIC_{ATCC\ 49230}$ < 0.50 µg/mL), enabling a more rigorous evaluation of our approach (Supp. Fig. S1).

Biocompatibility of LbL coatings

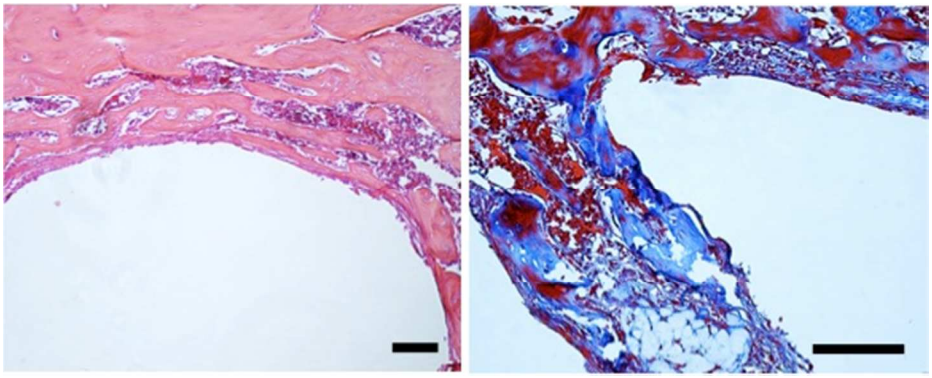

Fig. S2. Biocompatibility of the dual therapy LbL multilayer coatings in uninfected rats. H&E (Left) and Masson's trichrome (Right) sections of tibiae treated with BG coated implants at 2 weeks after implantation. Sections were viewed under bright-field microscopy. Scale bars, 100 μm.

We used a rat tibia defect model with no bacterial infection to examine the biocompatibility of LbL multilayer coatings. As shown in Supp. Fig. 2, we observed no apparent local toxicity or inflammation in any of the rats treated throughout these studies.

Surface morphology of LbL coatings

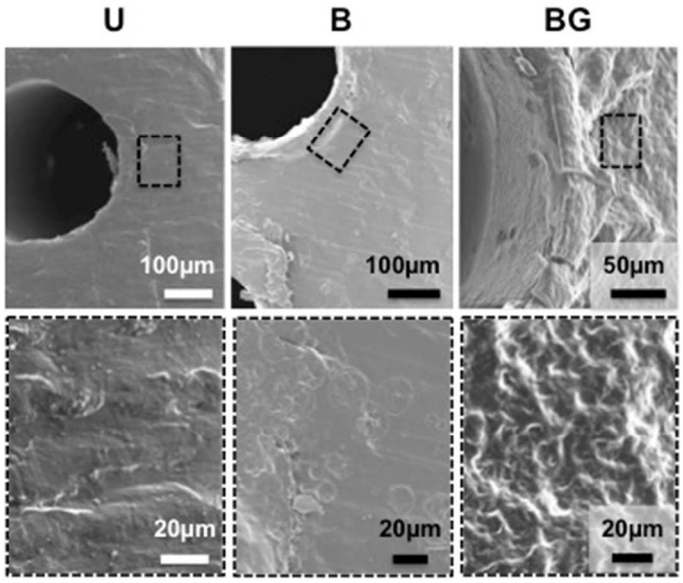

Fig. S3. Surface morphology of LbL coatings on drilled PEEK implants. SEM images of uncoated (U), B_{10} (B), and $B_{10}G_{20}$ (BG) coated implants.

Rough estimation of drug concentrations *in vivo*

We assumed that the effective control volume is the bone marrow space ($V_{\text{eff}} \sim 0.1$ mL) measured using μCT data. The conservation equation for drug mass M in the control volume can be written as

$$\frac{d}{dt}\int C\, dV = -\dot{M}_{\text{out}} + \dot{M}_{\text{release}}(t)$$

$$\frac{dM}{dt} = -\dot{M}_{\text{out}} + \dot{M}_{\text{release}}(t)$$

where C is the concentration of drug, $\dot{M}_{\text{out}}$ is the rate of drug cleared by blood vessels or consumed by cells, $\dot{M}_{\text{release}}$ is the rate of drug release from the implant, and t is time. For the sake of simplicity, we lumped the clearance rate from the target *via* blood circulation and uptake rate by cells and varied the value from 10 to 90% of drug mass in the control volume per time (i.e., $\dot{M}_{\text{out}}(t) = 0.1\sim0.9\, M(t)$).

The average concentration of drug $C_{\text{avg}}(t) = M/V_{\text{eff}}$ can be determined by numerically solving the semi-empirical differential equations with the initial condition $C_{\text{avg}}(0) = 0$ and $\dot{M}_{\text{release}}(t)$ from our *in vitro* release data (with implant surface area of 0.25 cm^2) in Fig. 2.

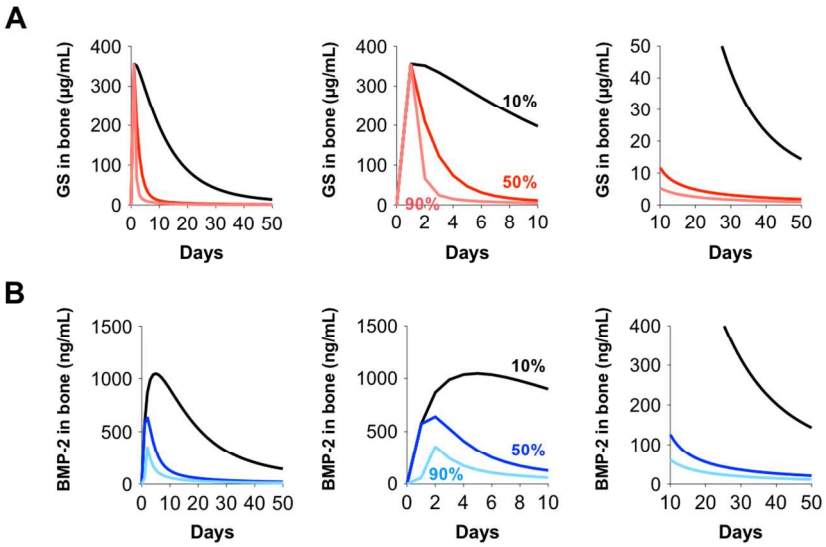

Fig. S4. Predicted concentration of GS and BMP-2 in bone. (A) Estimated concentration of GS from drilled PEEK implants coated with B_{10} + G_{20} with different clearance rate (black: 10%, red: 50%, salmon: 90%). (B) Estimated concentration of BMP-2 from drilled PEEK implants coated with B_{10} + G_{20} with different clearance rate (black: 10%, blue: 50%, sky blue: 90%).

Release kinetics

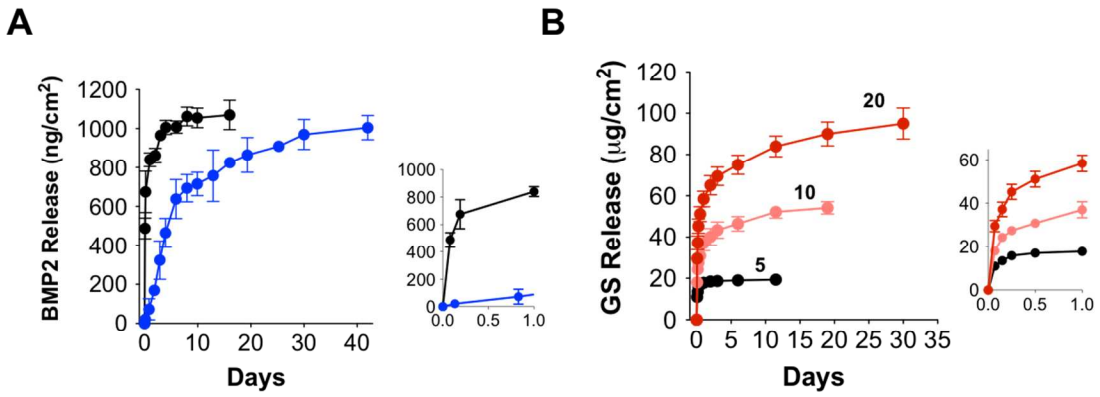

Fig. S5. Release kinetics and *in vitro* biological evaluation. (A) Cumulative release profiles of BMP-2 from drilled PEEK implants coated with B_{10} (●) or B_{10} + G_{20} composite (●). (B) Cumulative release profiles of GS from drilled PEEK implants coated with G_X where X = 5 (●), 10 (●), and 20 (●). Data represent the mean ± s.e.m., *n* = 3.

To test LbL film release, composite B_{10} + G_{20} (BG) deposited on PEEK implants were immersed in pH 7.4 PBS for varying times *in vitro* and GS or BMP-2 were quantitated by liquid scintillation counting and enzyme-linked immunosorbent assay (ELISA), respectively. The coating architecture and release kinetics of the two drugs (BMP-2 and GS) could be easily tailored by varying the number of deposited layers.

In vitro bioactivity evaluation

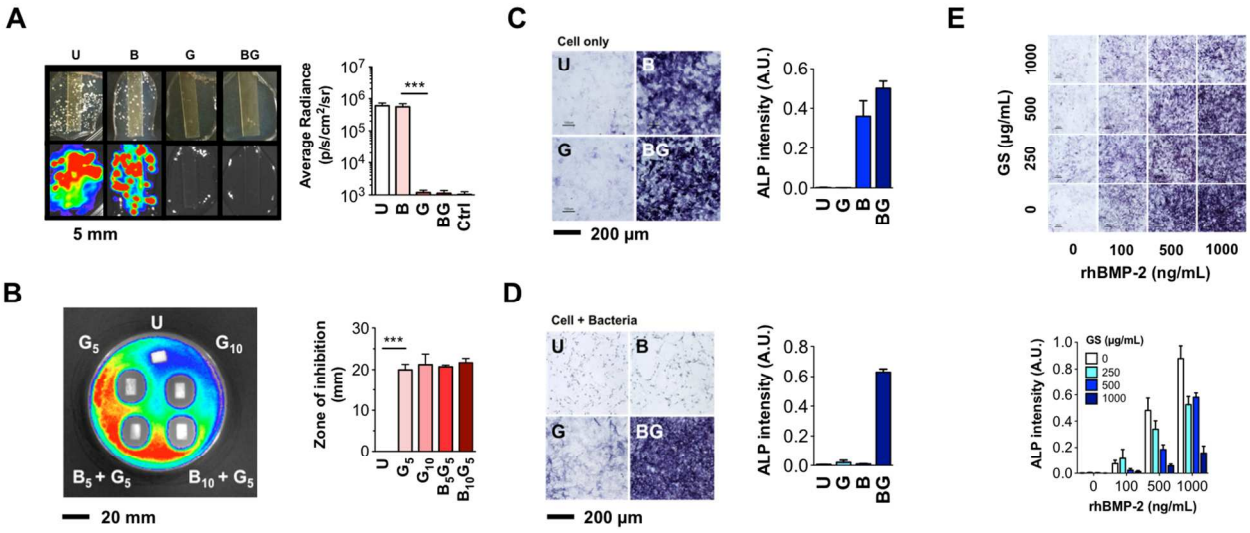

Fig. S6. *In vitro* bioactivity evaluation. (A) Representative bright-field (top) and bioluminescent (bottom) images from media-borne assay with *S. aureus* Xen 29 (Xen 29 SA). PEEK substrates uncoated or coated with B_{10} are colonized by bacteria (light beige colored dots in bright-field); substrates coated with G_{10} or $B_{10}G_{10}$ show no sign of colonization by bacteria. (B) Representative bioluminescent image from Kirby-Bauer assay showing the antibacterial activity of PEEK substrates coated with either GS only or a combination of GS and rhBMP-2. All coated substrates produce similar zones of inhibition (ZOI) of 20.0 mm against luciferase-expressing Xen 29 SA while the uncoated substrate (top) is completely colonized. (C) Alkaline phosphatase (ALP) colorimetric assay at day 6 on MC3T3-E1 cells differentiated with different release formulations (G_{20}, B_{10}, or $B_{10}G_{20}$) confirms the osteoinductive activity of BMP-2. (D) ALP staining of Xen 29 SA and MC3T3-E1 co-culture treated with GS in combination with BMP-2 released from different films (G_{20}, $B_{10,}$ or $B_{10}G_{10}$) at day 9. (E) Visual inspection of cultures after alkaline phosphatase (ALP) staining shows dose dependent activity of rhBMP-2 at different concentrations of GS. Data represent the mean ± s.e.m., *n* = 3–4. ***P < 0.001, analysis of variance (ANOVA) with a Tukey post hoc test.

As shown in Fig. S6A–B, GS-containing coatings (group G and BG) successfully prevented bacterial colonization on the surface and inhibited bacterial growth in the surrounding area, whereas bacteria completely overtook the uncoated and B coated substrates, resulting in 4 orders of magnitude higher bioluminescent signals. The MIC of the antibiotic remains unchanged following release, indicating the ability to retain drug activity within the films. To determine whether controlled BMP-2 release from the coatings would create a favorable osteogenic environment, we used alkaline phosphatase (ALP) activity assays with pre-osteoblast MC3T3-E1 cells, as ALP is an early marker of induction of bone differentiation. The cells treated with the multilayers releasing BMP-2 showed significant levels of ALP signal, demonstrating the onset of osteoinduction (Fig. S6C). We also validated that, when delivered together in co-cultures of *S. aureus* and MC3T3-E1 cells—a better representation of the *in vivo* scenario—GS and BMP-2

maintain their primary functions as an antibiotic and a growth factor respectively (Fig. S6D). There is no apparent cytotoxicity associated with the LbL films at these concentrations; however, exposing cells at elevated levels of GS (> 300 μg/mL) over a week resulted in reduced ALP signals, most likely due to its cytotoxic effects (Fig. S6E).

Rodent model of implant-related infection

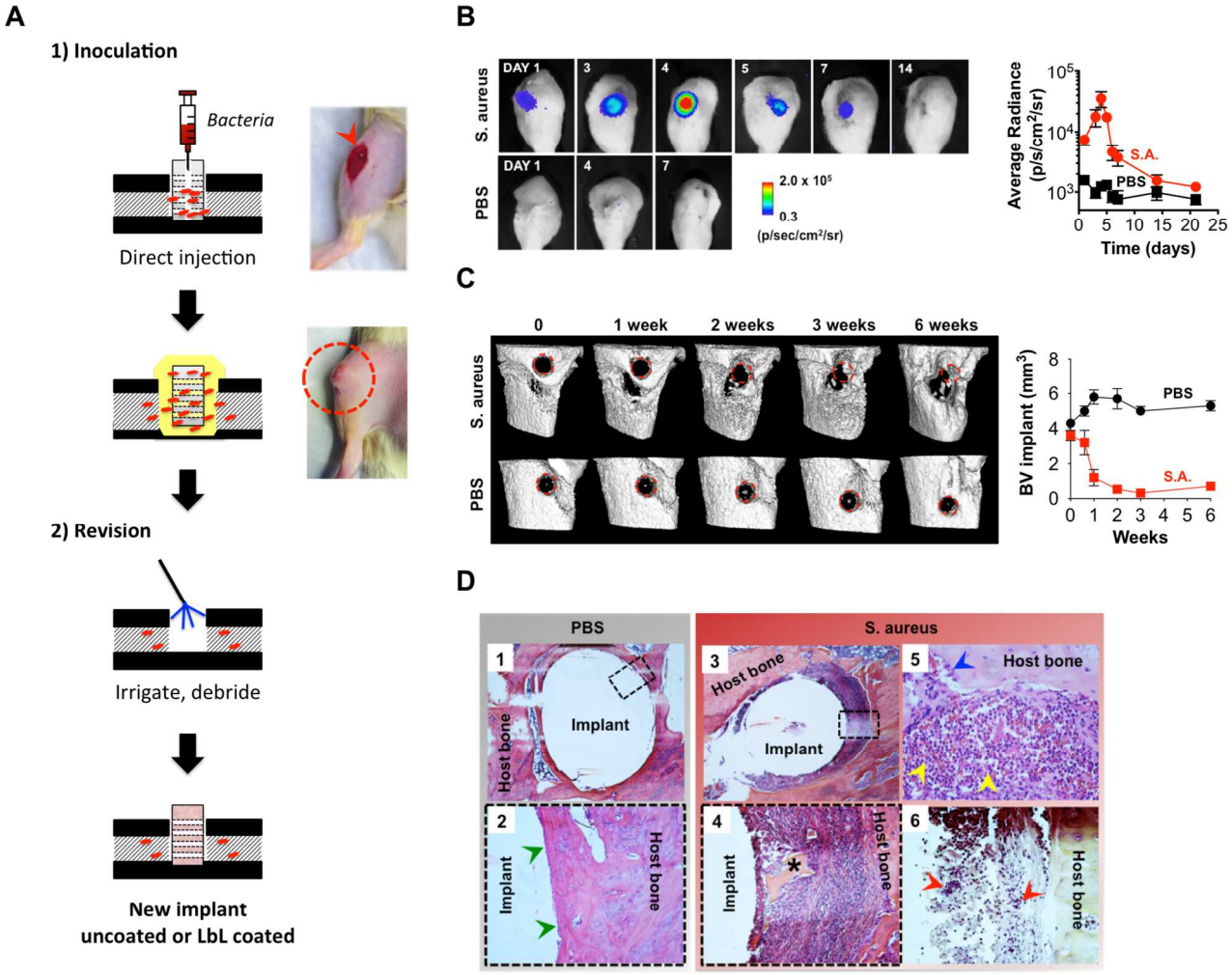

Fig. S7. Development of implant-related chronic osteomyelitis *via* direct inoculation method. (A) Groups of male rats were subjected to experimental implant-related osteomyelitis *via* direct inoculation of either *S. aureus* or sterile PBS (mock) in the channels of drilled implants. (B) Bacterial growth of bioluminescent-labeled *S. aureus* was tracked *in vivo* during the establishment of chronic osteomyelitis by monitoring the average radiance of *S. aureus* at the implant site over time. Data represent the mean ± s.e.m., *n* = 3. (C) Medial views of 3D reconstructed microCT images of representative tibiae at predetermined time points that received direct inoculation of either *S. aureus* or sterile PBS (mock) and imaging analysis of bone volume around the implants. Data represent the mean ± s.e.m., *n* = 3. (D) Histological sections of mock-infected implants (1–2) or *S. aureus* infected (3–6) at 3 weeks post-inoculation at low and high magnification. Scale bars, 200 μm (i–iv) and 200 μm (v–vi). Arrows: blue, osteoclasts; cyan, neutrophils; orange, macrophages; green, osteocytes; lime, osteoblasts; red, *S. aureus*.

Bacterial resistance test

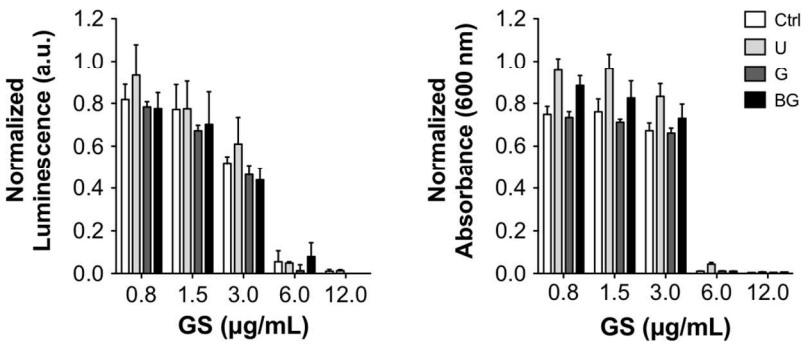

Fig. S8. Bacterial resistance against GS after explantation. *S. aureus* was collected from excised bone treated with different coatings, and its resistance against GS was measured upon exposure to serial dilutions of naked GS using bioluminescent imaging (left) and microplate reader at 600 nm (right). Original *S. aureus* Xen 29 served as control. MIC values for all groups were ~6 µg/mL, demonstrating no development of antibiotic resistance over time. Data represent the mean ± s.e.m., *n* = 3.

MIC values of GS against *S. aureus* Xen 29 isolated from untreated (U) and treated (G and BG) tibiae were measured to be identical to the parental strain (6 µg/mL, Ctrl), confirming no development of antibiotic resistance over time.

Histology

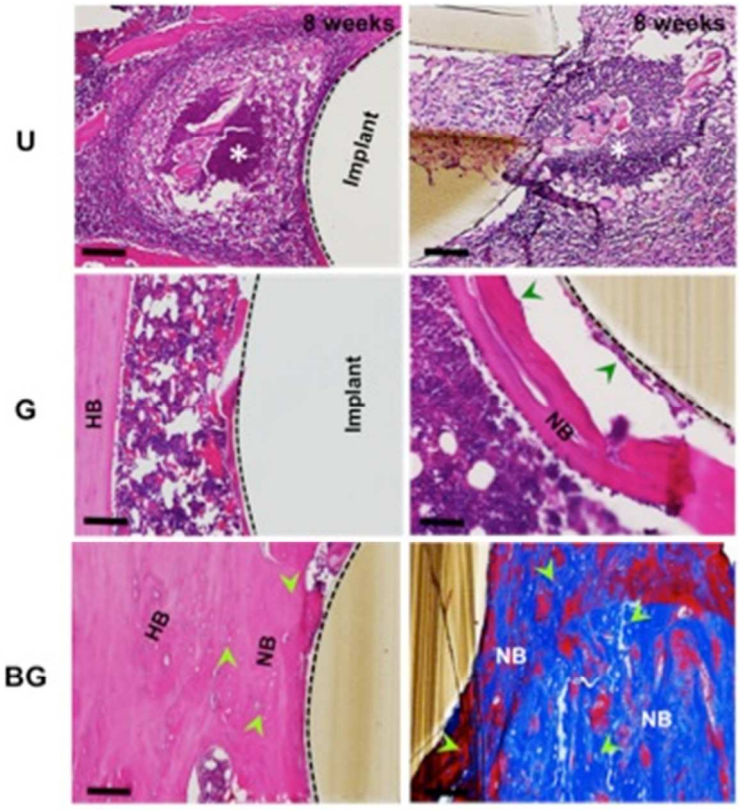

Fig. S9. Histological examination of excised tibiae treated with different coating formulations. (a) Hematoxylin and eosin (H&E) or Masson's Trichrome sections of representative tibiae treated with implants uncoated (U) or coated with G or BG at 8 weeks after revision. Sections were viewed under bright-field microscopy. Scale bars, 200 μm. Arrows: blue, osteoclasts; cyan, neutrophils; orange, macrophages; green, osteocytes; lime, osteoblasts; red, *S. aureus*.

The new bony tissue formed with hybrid BG layers was mature, organized, and cohesive enough to establish mechanical integrity of the reconstructed bone and implant, whereas no or very limited bone was regenerated with the uncoated or single-drug G coated, resulting in a lower stiffness and thus premature failure.

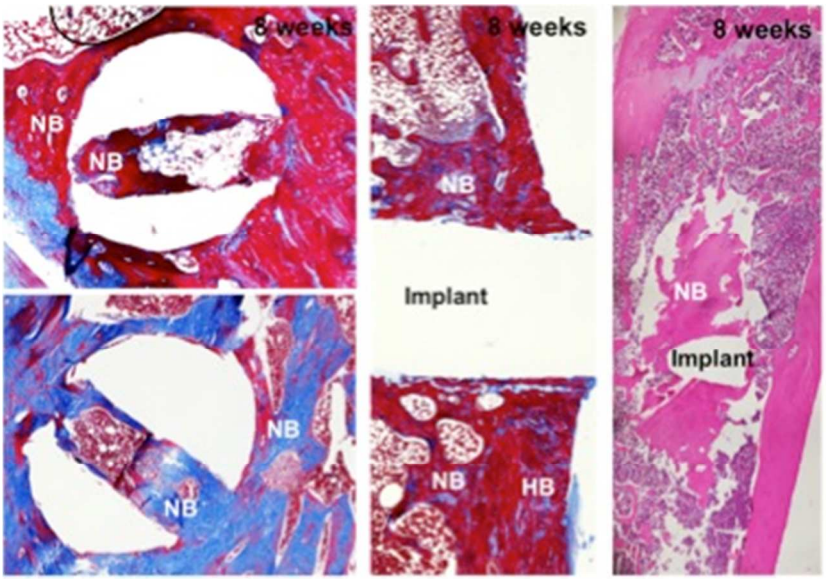

Fig. S10. Mature bone formation around implants coated with Dual therapy films. Masson's Trichrome and H&E sections of tibiae treated with implants coated with BG at 8 weeks after revision. Sections were viewed under bright-field microscopy. NB: new bone, HB: host bone.

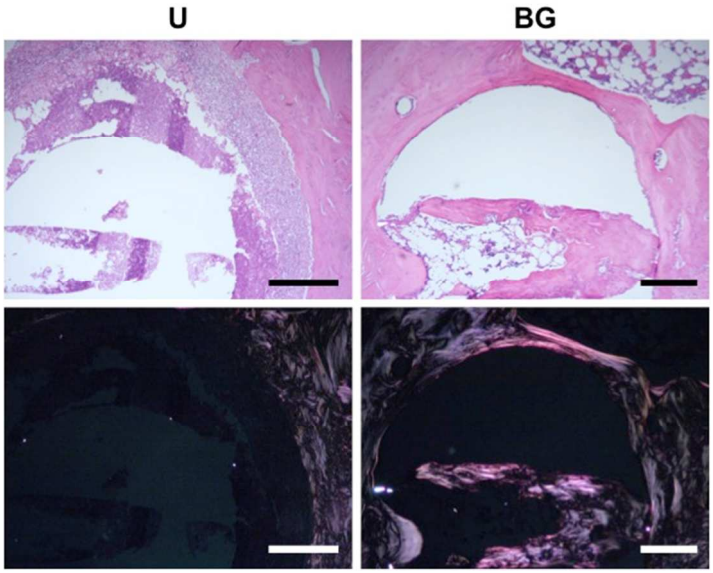

Fig. S11. Arrangement of new bone on uncoated (U) and Dual therapy coated (BG) PEEK implants at 8 weeks post-revision. (Left) There was no collagen fibril in the periprosthetic space. (Right) Mature, aligned collagen fibrils in the new bone were observed in the periprosthetic space. New bone is laid down as lamellar bone, with collagen fibrils nearly parallel, which takes longer to make but much stronger than premature woven bone. Regeneration of bone tissue was conformal to the implant shape (also conformal within the implant pores). Scale bars, 250 μm.

Bone exhibits positive form birefringence dominated by and dependent upon the orientation of its collagen. The biomechanical efficacy of bone as a tissue is largely determined by collagen

fibers of preferred orientation and distribution. Longitudinal fibers and crystallites, oriented more parallel to the long axis of the bone, are better able to resist tensile forces. Therefore, lamellar features of the newly synthesized bone around implants coated with the BG indicate bone maturation and restoration of most of the bone's original strength.

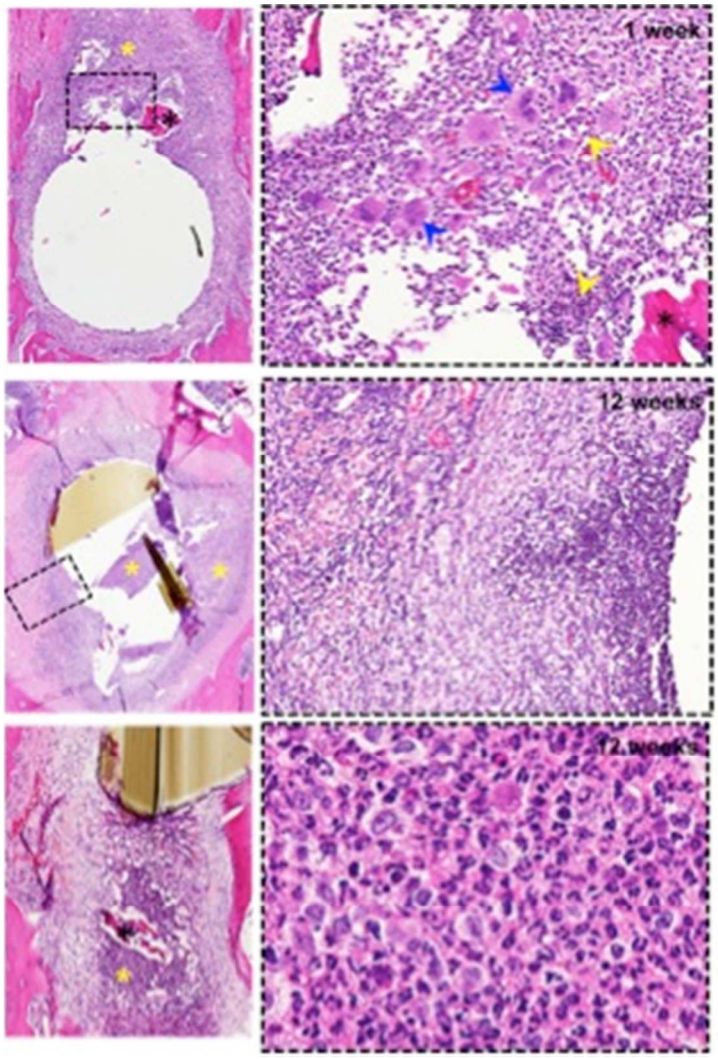

Fig. S12. Reinfection after revision in untreated rats. H&E sections of tibiae untreated (U) at 1 and 12 weeks after revision. Sections were viewed under bright-field microscopy high (left) and low (right) magnification. Arrows: blue, osteoclasts; cyan, neutrophils; orange, macrophages; green, osteocytes; lime, osteoblasts; red, *S. aureus*.

Tissue regeneration: imaging and quantification of new bone formation

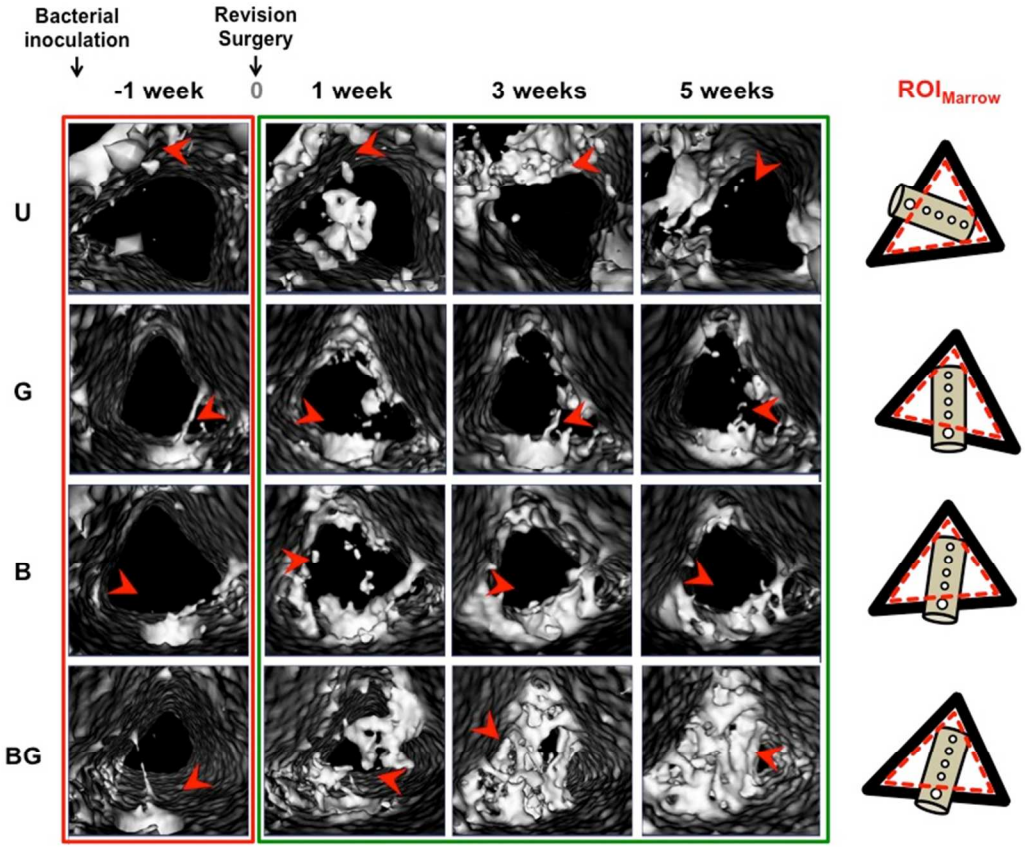

Fig. S13. New bone formation in medullary canal over time. 3D reconstruction of bone forming around implants with different formulations (U, G, B, and BG) within medullary canal at bacterial inoculation (-1) and 1, 3, and 5 weeks after revision, using ROIs marked by red dotted triangles shown in the drawings (right). Red arrows denote implant sites.

The volume and coverage of new bone around implants coated with G or BG generally increased over time, but much faster bone deposition and remodeling was observed on the implants coated with BG than others ($P < 0.01$); bone coverage of the BG hybrid coatings reached >80% in 3 weeks. In contrast, the untreated (U or B) showed significantly less bone formation.

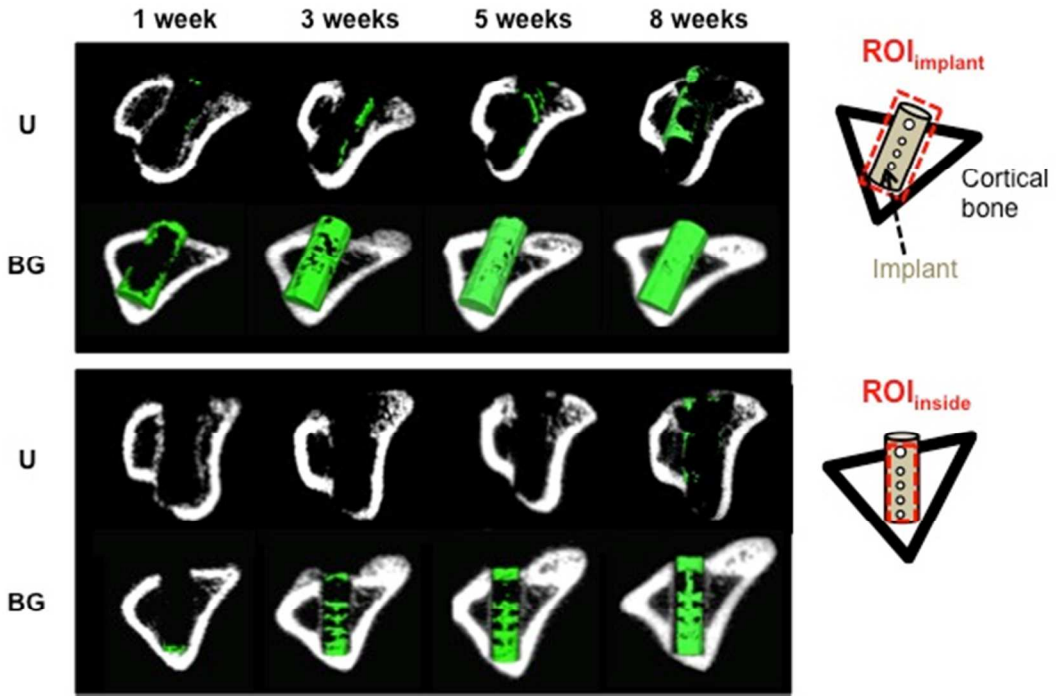

Fig. S14. New bone formation around and inside the drilled implants. (Top) Radiographs and 3D reconstruction of bone forming around (top) and inside the channels (bottom) of drilled implants with different formulations (U vs. BG) at 1, 3, 5, and 8 weeks after revision, using cylindrical ROIs marked by red dotted boxes shown in the drawings (right).

We observed complete bone coverage and penetration into the channels of the BG coated by 8 weeks after revision, confirming that controlled BMP-2 release is highly effective at enhancing osseointegration and optimizing the implant-tissue interface.

Pull-out testing

Table S1. Interfacial shear strength (MPa) of implants coated with different film formulations. Strengths were calculated by pull-out force data from in Fig. 5h. Data are means ± s.e.m. (*n* = 3–4).

Group	3 weeks	5 weeks	8 weeks
U	0.027 ± 0.010	0.051 ± 0.010	0.13 ± 0.064
G	0.092 ± 0.035	0.30 ± 0.083	0.45 ± 0.10
BG	0.28 ± 0.033	0.79 ± 0.040	1.2 ± 0.15